

Three-Dimensional Microwave Holography Based on Broadband Huygens' Metasurface

Zhuochao Wang,^{1,2} Jian Liu,¹ Xumin Ding^{1,2,4,*} Weisong Zhao,¹ Kuang Zhang,^{2,4,†} Haoyu Li,^{1,‡} Badreddine Ratni,³ Shah Nawaz Burokur^{1,§}, and Qun Wu²

¹ Advanced Microscopy and Instrumentation Research Center, Harbin Institute of Technology, Harbin 150080, China

² Department of Microwave Engineering, Harbin Institute of Technology, Harbin 150001, China

³ LEME, UPL, Univ Paris Nanterre, F92410 Ville d'Avray, France

⁴ Key Laboratory of Millimeter Waves, Nanjing 210096, China

(Received 1 August 2019; revised manuscript received 10 November 2019; published 21 January 2020)

Benefiting from prominent performance in various scientific fields, metasurface research has been flourishing over the past decade. Huygens' metasurface, as an emerging subcategory of metasurface, can theoretically achieve full control of electric field distribution within the subwavelength scale. Driven by its outstanding manipulation capacity, the three-dimensional holography utilizing broadband Huygens' metasurface is demonstrated in the microwave regime in this paper. For the broadband working properties, two types of equivalent circuit are integrated into the design of Huygens' meta-atom. Besides, for high image quality, the modified weighted Gerchberg-Saxton (GSW) algorithm is implemented for specific interfacial phase distribution. The proof-of-concept experiments show notable microwave holographic images, with an 86.2% transmittance efficiency, a 62.7% imaging efficiency, and an 88.1 signal-to-noise ratio at 12 GHz. The proposed holography extends the route to broadband microwave applications in security, data storage, and antenna systems.

DOI: 10.1103/PhysRevApplied.13.014033

I. INTRODUCTION

Digital holography, a promising paradigm of imaging technology, can reconstruct fictitious objects with a desired intensity and phase information [1]. Traditional holograms are created by recording interference patterns between the light scattered by the object in real space and the coherent reference beam [2,3]. Instead of cumbersome devices and sophisticated equipment, digital holography achieves reconstruction of a hologram by directly producing the interference wave front according to diffraction theory. Conventionally, digital holography relies on phase accumulation through propagation generated by changing either the thickness or the refractive index of the material layer [4]. However, it faces the challenges of low-resolution imaging, high-order diffraction, and a complex fabrication process [5]. As nanofabrication technology progresses, the emerging metasurface technology can provide spatially varying phase discontinuities within the subwavelength scale. As an ensemble of the elaborately

designed meta-atom array, metasurfaces present a broad range of applications in directional radiators [6,7], planar lenses [8], vortex-beam generators [9–11], thin-film cloaking [12], and digital holograms [13,14]. Metasurface holography can significantly improve the image quality and robustness against fabrication tolerances [15–17]. However, the design of metasurfaces mainly depends on the theory of symmetric and asymmetric resonances [18] or Pancharatnam-Berry phase elements [19,20], which hardly satisfy the indices of both a high transmittance efficiency and a broadband working range simultaneously.

The concept of Huygens' metasurface presents an improvement in transmittance efficiency and phase coverage. By integrating orthogonal electric and magnetic dipoles into each meta-atom, Huygens' metasurfaces can fully control the amplitude and phase of transmission and reflection coefficients [21]. There is always a trade-off between the manipulation efficiency and the operating bandwidth in the different designs of microwave-transmission-type metasurfaces. For multilayer metasurfaces [22], a higher number of layers can compensate a larger phase-delay variation and achieve a wider bandwidth but results in much greater energy losses. An alternative solution is a metasurface designed from Pancharatnam-Berry (P-B) phase elements, which can

*xuminding@hit.edu.cn

†zhangkuang@hit.edu.cn

‡lihaoyu@hit.edu.cn

§sburokur@parisnanterre.fr

ensure broadband functionality and a full phase shift of the cross-polarized transmitted wave. However, its cross-coupling efficiency cannot be more than 25% in theory from a single-layered metasurface [23]. In contrast, Huygens' metasurface can balance the above contradictory factors by elaborately designing the resonance properties of electric and magnetic dipoles. Hence, Huygens' metasurface opens the door to solving the limitations of conventional metasurface design and has been applied to versatile research fields, such as beam refraction [24], focusing [25,26], beam shaping [27,28], and three-dimensional (3D) imaging with depth retrieval [29].

Here we propose and experimentally realize a 3D holographic imaging technique utilizing a broadband Huygens' metasurface. By modulating the overlap of the electric and magnetic resonances, 16 Huygens' meta-atoms with a 2π transmission-phase range are arranged to produce the phase profile obtained by the modified holographic Gerchberg-Saxton (GSW) algorithm. As shown in Fig. 1, the Huygens' metasurface hologram, composed of 77×89 meta-atoms, is elaborately designed for the holographic imaging of a 3D inverted pyramid, which can be segmented into three subplanes at different focal lengths. In particular, compared to the optical holograms of 800×800 pixels [16], the total physical dimensions of microwave holograms limit the amount of components due to the relatively large working wavelength. If the total quantity of Huygens' meta-atoms swells to the same order of magnitude as the optical hologram, more sophisticated patterns containing thousands of focal points can be realized, which can be regarded as giving a true sense of 3D holography, instead of discrete multiplane imaging. Hence,

the Huygens' metasurface holography proposed here is a proof-of-concept experiment to verify the feasibility of the designed scheme and estimate the image quality. According to the experimental results, the designed 3D microwave holographic imaging can be observed in a broadband bandwidth, in which the efficiency and quality of the imaging are maintained at a high level. Compared to our previous study on metasurfaces encoded with a designated phase profile for a single two-dimensional pattern [30], the proposed scheme can integrate three diverse holographic images into a single Huygens' metasurface design, with the merit of a larger information capacity. Overall, the subwavelength Huygens' meta-atoms promise the efficient manipulation of transmitted microwave low-noise interference, high-spatial resolution, and high-density information storage of reconstructed multiplane images, opening the way toward microwave holography with high performance.

II. DESIGN OF HUYGENS' METASURFACE HOLOGRAPHY

Microwave digital holography can be generated by encoding phase profiles into a set of Huygens' meta-atoms. Huygens' metasurface can be regarded as the physical implementation of Huygens' principle through the use of a metasurface. By integrating designated electric and magnetic dipoles into meta-atoms, an arbitrary wave front can be realized under normal incidence [31]. For full coverage of the required transmission phase, the design of Huygens' metasurface incorporates two types of meta-atom. Figures 2(a) and 2(b) illustrate two basic structures of transmission-type Huygens' meta-atoms with the same period and thickness. A split-ring resonator on one side of the meta-atom plays the role of a magnetic dipole with a surface current flowing in a loop. On the other side, the *LC* series resonator operates as an electric dipole with the main surface current flowing along the resonator. The manipulation of the transmitted electric field is based on the modulation of the resonant overlap induced by the electric and magnetic dipoles [32]. For low transmitted energy losses and a broad operating bandwidth, the relative permittivity of the dielectric substrate is first chosen as 2.2 to decrease the value of the resonant quality factor. Second, since the decrease of the capacitance in the equivalent circuit in Fig. 2(a) leads to an evident increase of the value of the quality factor, the shunt-capacitor circuit model is added to the traditional Huygens' meta-atom design to keep the equivalent capacitance at a high value. Therefore, the single and shunt capacitance can guarantee both a relatively low quality factor and a sufficient modulation range of the electric resonance property. By appropriately changing the lengths l_e and l_m , the overlap of the electric and magnetic resonances can be adjusted for the designated operating bandwidth and transmission

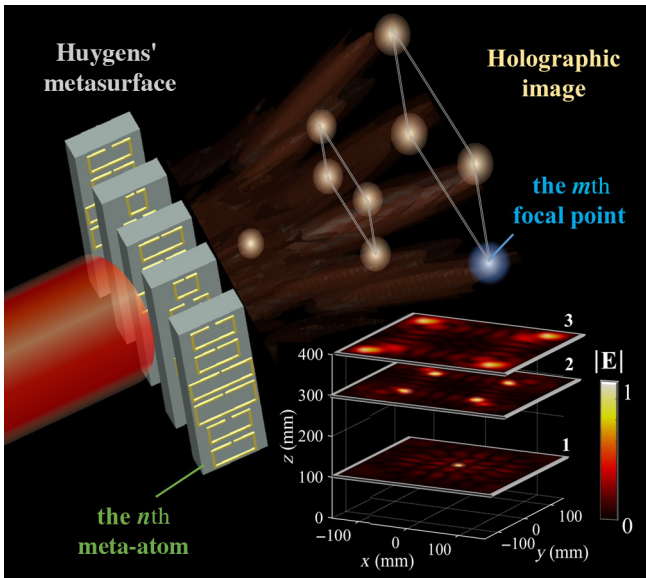


FIG. 1. A schematic diagram of the hologram structure and the reconstruction procedure of the microwave 3D imaging utilizing Huygens' metasurface.

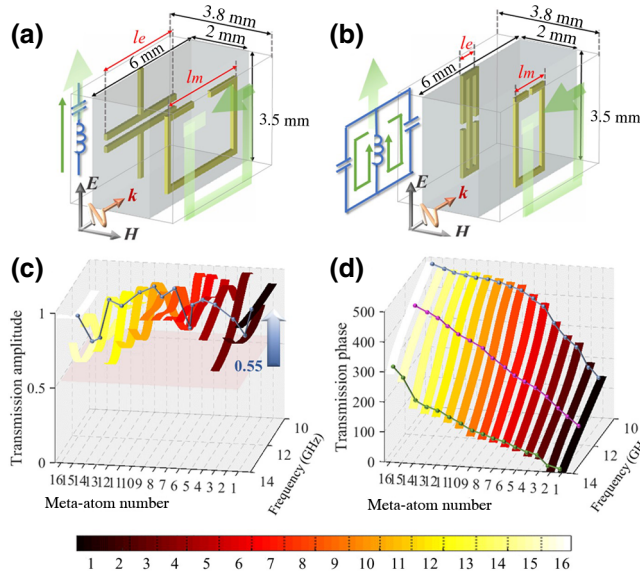


FIG. 2. The design of the transmission-type Huygens' meta-surface. (a),(b) Schematic views of the proposed Huygens' meta-atoms and the simulated surface current along the metallic patches on both sides of the dielectric substrate ($\epsilon_r = 2.2$, $\tan\delta = 0.002$). (c),(d) The simulation results of 16 extracted meta-atoms with different geometrical parameters, l_m and l_e . Each stripe indicates the transmission amplitude (c) and transmission phase (d) of each meta-atom. In particular, the green, purple, and blue dotted lines in (d) illustrate the same phase step among the 16 meta-atoms at 10, 12, and 14 GHz, respectively.

phase coverage. Figures 2(c) and 2(d) show the simulation results obtained from the CST MICROWAVE STUDIO commercial software. A group of 16 meta-atoms with two basic types of equivalent circuit model is extracted, for use as holographic construction components. The transmission-phase coverage reaches 2π and the transmission amplitude stays above 0.55 within the 10–14 GHz operating frequency range. The phase shift is quantified as high as 16 values to optimally fit the continuous phase mapping of the hologram and reduce the undesired coupling effect between adjacent meta-atoms. As illustrated in Fig. 2(d), although the transmission phase varies with frequency, the phase step stays approximately the same over the whole band of interest with a relatively high transmission amplitude, especially at 12 GHz. These characteristics obtained from Huygens' meta-atoms further demonstrate the wider phase-shift coverage than multilayer structures [22] and the higher manipulation efficiency than metasurfaces using the P-B phase mechanism [23]. Therefore, the proposed Huygens' metasurface can make an excellent trade-off between transmission efficiency and phase-shift variation in the microwave regime. Moreover, due to the low quality factor of resonance, the transmission-phase shift induced by the oblique incidence is relatively consistent among the proposed 16 meta-atoms, which enables holographic

imaging over a wide range of incidence angles. More details can be found in the Supplemental Material [33].

The next step is the achievement of 3D microwave holography with the proposed Huygens' meta-atoms. The modified weighted GSW algorithm is adopted here to obtain the holographic phase distribution [34,35]. Instead of directly calculating the desired wave front, the GSW algorithm constructs an iterative loop between the imaging object and the hologram plane via the propagating function to optimize image performance and decrease the electric field intensity differences among the foci step by step. Moreover, due to the limited focal length with respect to the microwave wavelength, the function of the electromagnetic propagation is modified as a Green's function instead of the traditional Fraunhofer diffraction generally used in the optical regime [30]. Figure 1 shows the hologram structure and theoretical reconstruction procedure of the 3D imaging utilizing the modified GSW algorithm. E_m is defined here as the electric field intensity of the m^{th} ($m = 1, \dots, M$) focal point and ϕ_n denotes the phase shift of the n^{th} ($n = 1, \dots, N$) meta-atom under normal incidence. The iteration algorithm proceeds as follows:

$$w_m^p = w_m^{p-1} \frac{\langle |E_m^{p-1}| \rangle}{|E_m^{p-1}|} \quad (m = 1, \dots, M), \quad (1)$$

$$\phi_n^p = \arg \left(\sum_{m=1}^M \frac{e^{ikr_n^m}}{r_n^m} \frac{w_m^p E_m^{p-1}}{|E_m^{p-1}|} \right) \quad (n = 1, \dots, N), \quad (2)$$

where r_n^m is the distance between the n^{th} meta-atom and the m^{th} focal point and superscript p represents the p^{th} iterative step. $\langle |E_m^{p-1}| \rangle$ denotes the average focal intensity in the $(p-1)^{\text{th}}$ step. According to Eqs. (1) and (2), the weight factor w_m is introduced to reduce the intensity differences among the M foci. In particular, the initial condition is set as

$$w_m^0 = 1, \quad \phi_n^0 = \frac{2\pi n}{N}. \quad (3)$$

The lower-right quadrant in Fig. 1 illustrates the theoretical 3D holographic imaging at 12 GHz based on the proposed modified GSW algorithm. The calculated results verify that the GSW-based holography can achieve focal uniformity and high image quality.

III. EXPERIMENTAL CHARACTERIZATION OF HUYGENS' METASURFACE HOLOGRAPHY

To investigate the performance of the proposed Huygens' metasurface holography, a 3D image is designed to project onto different planes ($z_1 = 125$ mm, $z_2 = 300$ mm, and $z_3 = 400$ mm, respectively) at 12 GHz. Based on the modified GSW algorithm, the required phase

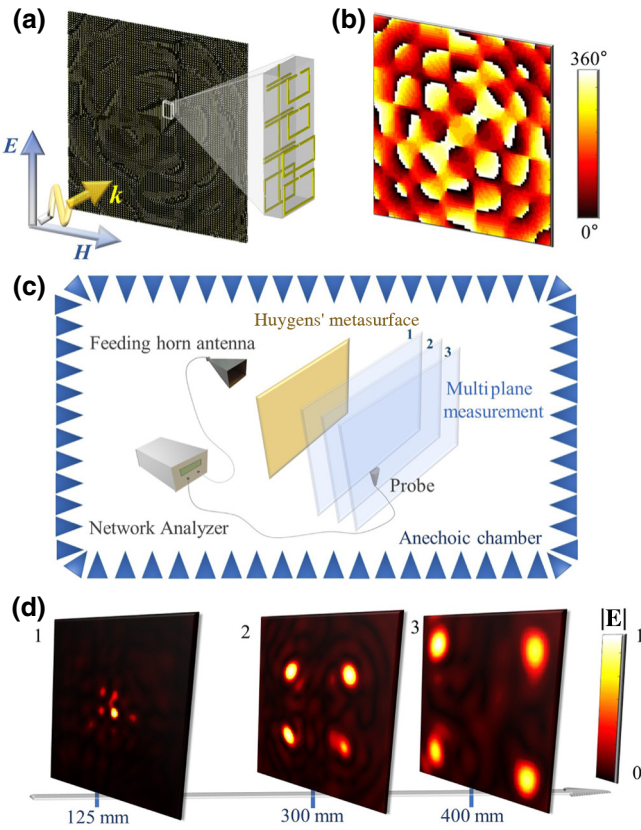


FIG. 3. The design of the hologram based on the modified GSW algorithm. (a) The overall hologram pattern of the constituent meta-atoms. (b) The calculated phase distribution. (c) The experimental setup for measuring the Huygens' metasurface hologram. (d) The simulation results of the 3D holographic imaging at 12 GHz.

profile for imaging is encoded into the Huygens' metasurface. Figures 3(a) and 3(b) depict the overall hologram pattern of the constituent meta-atoms and the calculated phase map under normal incidence, respectively. The hologram covers an area of $310 \text{ mm} \times 310 \text{ mm}$ with 77×89 meta-atoms. As a proof of concept of the proposed holography, the Huygens' metasurface sample is fabricated using a commonly used printed circuit board in the microwave domain and experimentally measured.

For quantitative evaluation of the holography, three parameters are adopted here. To describe the transmission property of Huygens' metasurface over the frequency bandwidth, the transmittance efficiency is defined as the ratio of the total transmitted energy to the incident energy within the size of Huygens' metasurface [36]. To characterize the image quality, the signal-to-noise ratio (SNR) is introduced as the ratio of the peak intensity in the image to the standard deviation of the background noise [37]. Besides, the imaging efficiency is assumed to be the fraction of the focal intensity referenced to the transmitted intensity in the imaging plane [38]. In particular,

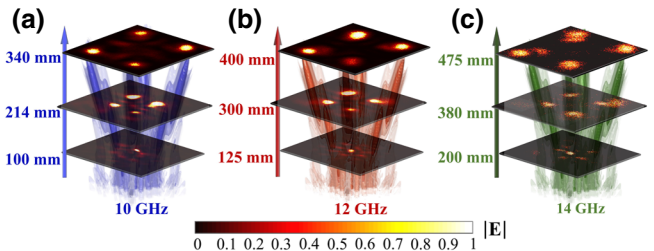


FIG. 4. The experimental results of the electric field intensity distribution in three planes: (a) 12 GHz; (b) 10 GHz; (c) 14 GHz.

evaluate the total performance of multiplane holographic imaging, the above parameters are calculated as the average of each imaging plane. For the experimental validation measurements, the setup consists of a feeding horn antenna to provide the quasiplane wave incidence of the holographic Huygens' metasurface sample and of a near-field probe to measure the transmitted electric field point by point, as illustrated in Fig. 3(c).

Figure 3(d) presents the results of simulations performed utilizing the CST MICROWAVE STUDIO commercial software and the image features agree well with the theoretical predictions. Moreover, Fig. 4(a) depicts the experimentally observed images at designated focal lengths for the frequency of 12 GHz. The transmittance efficiency reaches as high as 86.2%, proving the efficient manipulation capacity of the proposed Huygens' metasurface. The imaging efficiency is measured to be 62.7% and the value of SNR to be equal to 88.1, respectively. To highlight the characteristics of the holographic image obtained with our proposed concept, a comparison with other metasurface-based designs is carried out. Table I presents the experimental imaging parameters of some representative research studies on metasurface holography. Owning to the optimized phase algorithm, the refined transmission-phase step and few losses in transmission, the transmittance and imaging efficiency of the proposed scheme are obviously notable compared to other transmission-type metasurface holograms. In contrast, the last two designs in Table I illustrate the outstanding manipulation efficiency of reflection-type holographic imaging, due to the relatively simple design of the meta-atom, which commonly utilizes the metal film on the bottom face of the substrate as a perfect reflector.

Due to the broadband property of the proposed Huygens' metasurface, the 3D holographic imaging designed at 12 GHz can also be observed from 10 to 14 GHz, as shown in Figs. 4(b) and 4(c). In the working bandwidth, the phase step of Huygens' meta-atom is approximately constant, as shown in Fig. 2(d), while the phase accumulation along a specific propagation path varies with frequency. Therefore, the imaging performance is closely related to the working frequency. The in-plane four-focus imaging is first designed for analysis, as illustrated in Fig. 5. For

TABLE I. A summary of previous research studies on metasurface holography.

Reference	Working frequency (wavelength)	Type	Polarization	Transmittance (reflection) efficiency	Imaging (diffraction) efficiency	Overall efficiency
Ni <i>et al.</i> [4]	676 nm	Transmission	Linear	10%
Li <i>et al.</i> [38]	657 nm	Transmission	Insensitive	...	15.88%	...
Walther <i>et al.</i> [39]	905 nm	Transmission	Insensitive	4.1%	2.56%	0.11%
Wang <i>et al.</i> [40]	633 nm	Transmission	Circular	~50%	19%	~9.5%
Zhao <i>et al.</i> [41]	785 nm	Transmission	Insensitive	86%	23.6%	20.3%
Chong <i>et al.</i> [36]	1477 nm	Transmission	Insensitive	82%	40%	32.8%
This work	12 GHz	Transmission	Linear	86.2%	62.7%	54.0%
Li <i>et al.</i> [17]	7.8 GHz	Reflection	Linear	60%
Zheng <i>et al.</i> [14]	825 nm	Reflection	circular	94%	80%	75.2%

identical imaging over a broad frequency band, the focal length of each imaging plane varies with the operating frequency and the relationship between the location of the image and wavelength can be derived as $\lambda z = \text{constant}$ under the paraxial approximation [18]. Meanwhile, at the same focal length, the imaging pattern will be enlarged

with an increase in frequency, as can be clearly observed in Fig. 5(c). Based on the same approximation method, the magnification coefficient is inversely related to the operating frequency. The simple and direct description of the relationship between the imaging feature and the operating frequency shows good agreement with the theoretical reconstruction and simulation results.

Figures 4(b) and 4(c) present the experimentally observed 3D imaging results at the bandwidth edges of 10 and 14 GHz. The measured focal-length variation accords well with the above-derived equation $\lambda * z = \text{constant}$. The transmittance efficiencies are measured to be 75.1% and 68.6% at 10 and 14 GHz, respectively, proving the broadband manipulation of the proposed Huygens' metasurface. The imaging efficiencies are 49.6% and 47.3%. Additionally, the values of the SNRs are 83.7 and 85.0. Small deviations from the theoretical designs can be observed in the measured focal locations, since the fabrication tolerances of the permittivity and the geometric dimensions influence the electromagnetic response of Huygens' metasurface.

Overall, the measured results show that the designed 3D microwave holographic imaging can be observed over a broad frequency bandwidth, in which both the efficiency and the quality of the imaging are maintained at a high level. Hence, the prominent performance of the proposed Huygens' metasurface holography based on the modified GSW algorithm provides a promising route for the design and reconstruction of 3D imaging. Actually, the proposed holography can be regarded as the multipoint focusing utilizing the optimized algorithm and as subwavelength-scale control on the interface. In microwave communication, the focusing points in the near field, regarded as independent channels, can greatly satisfy the substantial demands of the emerging 5G technology for “huge capacity, huge connections, and extensive applications” [42]. Hence, the proposed holography offers a mechanism to help achieve more accurate and elaborate control of the microwave electromagnetic field, rather than the traditional far-field manipulation, which will make great sense in the fields of short-range communication, detection,

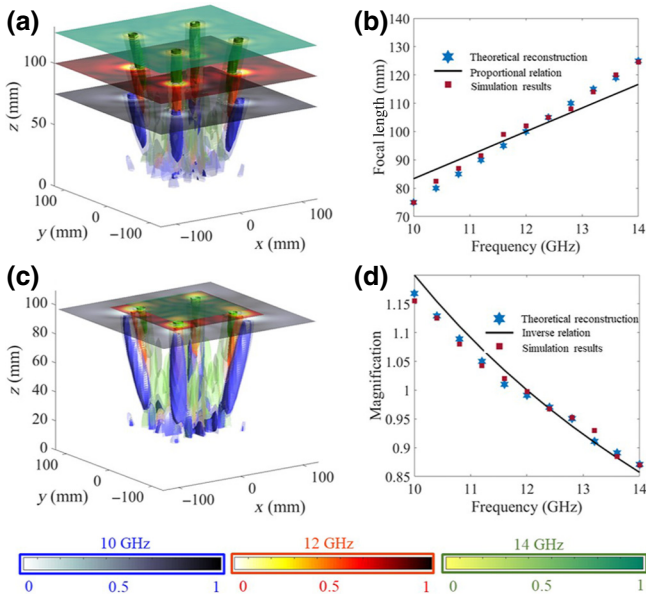


FIG. 5. Variation of the four-focus imaging performance with frequency. (a) A reconstruction of identical imaging at 10 GHz (blue), 12 GHz (red), and 14 GHz (green). (b) The focal length over the 10–14 GHz frequency range. The blue hexagrams denote the theoretical results based on microwave propagation of the Green's function. The red square dots represent the simulation results and the black curve is calculated based on the approximate proportional relation. (c) The imaging performance at the same focal length of 100 mm at 10 GHz, 12 GHz, and 14 GHz. (d) The magnification coefficient over the 10–14 GHz frequency range. The blue hexagrams denote the theoretical results, the red square dots represent the simulation results, and the black curve is calculated based on the approximate inverse relation.

security, data storage, and information processing. In particular, the broadband method of integrating slightly different equivalent circuits into Huygens' meta-atom designs and the analysis of the imaging feature variation with frequency can extend toward higher frequencies, such as the terahertz and optical regimes (details can be found in the Supplemental Material [33]). Moreover, the multi-plane images can be postprocessed with a state-of-the-art Hessian-matrix penalty for further optimization to achieve significant improvement of the image quality, as is shown in detail in the Supplemental Material [33].

IV. CONCLUSION

In conclusion, we demonstrate a 3D microwave holographic imaging over the 10–14 GHz frequency band with physical implementation and numerical processing. To overcome the restriction of a narrow operation bandwidth based on the resonance mechanism of Huygens' metasurface, equivalent circuit designs and a low substrate permittivity are adopted here to decrease the quality factors of the resonances. According to the simulation results, the transmission-phase range of the proposed Huygens' meta-atoms reaches 2π and the transmission amplitude stays above 0.55 within the 10–14 GHz frequency range, which demonstrates the relatively broadband and efficient features in the microwave regime compared to the designs of Refs. [22] and [23]. Next, 16 Huygens' meta-atoms are extracted to accomplish the phase map based on the modified GSW algorithm to realize the phase-encoded holograms, which can provide focal uniformity and high imaging performance. The obtained results agree well with the theoretical analysis and the characteristic parameters of the imaging, verifying the feasibility and potential applications of the proposed design scheme. The proposed Huygens' metaholography paves the way for 3D broadband display, beam shaping, smart antenna systems, and other broadband microwave applications. Besides, the introduction of amplitude manipulation will enable the additional functions on phase-only holography, such as artifact-free imaging and control of surface textures [43]. Moreover, the concept can be readily applied to other frequency ranges as well and implementations would be possible with suitable fabrication technologies.

ACKNOWLEDGMENTS

This work is supported by the National Natural Science Foundation of China (Grant No. 61701141), the Open project of the State Key Laboratory of Millimeter Waves (K202001), and the Fundamental Research Funds for the Central Universities (Grant No. HIT.NSRIF.2019029).

Zhuochao Wang and Jian Liu contributed equally to this work. This paper was written through contributions from all of the authors and all of the authors have approved the final version.

- [1] Myung K. Kim, *Digital Holographic Microscopy* (Springer, New York, NY, 2011), pp. 149–190.
- [2] J. Scheuer and Y. Yifat, Holography: Metasurfaces make it practical, *Nat. Nanotech.* **10**, 296 (2015).
- [3] U. Schanars, C. Falldorf, J. Watson, and W. Jueptner, *Digital Holography and Wavefront Sensing: Principles, Techniques and Applications* (Springer-Verlag, Berlin Heidelberg, Germany, 2015).
- [4] X. Ni, A. V. Kildishev, and V. M. Shalaev, Metasurface holograms for visible light, *Nat. Commun.* **4**, 2807 (2013).
- [5] W. Wan, J. Gao, and X. Yang, Metasurface holograms for holographic imaging, *Adv. Opt. Mater.* **5**, 1700541 (2017).
- [6] B. Ratni, A. de Lustrac, G. P. Piau, and S. N. Burokur, Reconfigurable meta-mirror for wavefronts control: Applications to microwave antennas, *Opt. Express* **26**, 2613 (2018).
- [7] Y. Yuan, K. Zhang, X. Ding, B. Ratni, S. N. Burokur, and Q. Wu, Complementary transmissive ultra-thin meta-deflectors for broadband polarization-independent refractions in the microwave region, *Photonics Res.* **7**, 80 (2019).
- [8] X. Chen, Y. Zhang, L. Huang, and S. Zhang, Ultrathin metasurface laser beam shaper, *Adv. Opt. Mater.* **2**, 978 (2014).
- [9] M. Q. Mehmood, S. Mei, S. Hussain, K. Huang, S. Y. Siew, L. Zhang, T. Zhang, X. Ling, H. Liu, J. Teng, A. Danner, S. Zhang, and C. W. Qiu, Visible-frequency metasurface for structuring and spatially multiplexing optical vortices, *Adv. Mater.* **28**, 2533 (2016).
- [10] Y. Zhang, W. Liu, J. Gao, and X. Yang, Generating focused 3D perfect vortex beams by plasmonic metasurfaces, *Adv. Opt. Mater.* **6**, 1701228 (2018).
- [11] K. Zhang, Y. Yuan, X. Ding, B. Ratni, S. N. Burokur, and Q. Wu, High-efficiency metalenses with switchable functionalities in microwave region, *ACS Appl. Mater. Int.* **11**, 28423 (2019).
- [12] M. Selvanayagam and G. V. Eleftheriades, Discontinuous electromagnetic fields using orthogonal electric and magnetic currents for wavefront manipulation, *Opt. Express* **21**, 14409 (2013).
- [13] Y. Yifat, M. Eitan, Z. Iluz, Y. Hanein, A. Boag, and J. Scheuer, Highly efficient and broadband wide-angle holography using patch-dipole nanoantenna reflectarrays, *Nano Lett.* **14**, 2485 (2014).
- [14] G. Zheng, H. Mühlenbernd, M. Kenney, G. Li, T. Zentgraf, and S. Zhang, Metasurface holograms reaching 80% efficiency, *Nature Nanotech.* **10**, 308 (2015).
- [15] A. Arbabi, Y. Horie, A. J. Ball, M. Bagheri, and A. Faraon, Subwavelength-thick lenses with high numerical apertures and large efficiency based on high-contrast transmitarrays, *Nat. Commun.* **6**, 7069 (2015).
- [16] L. Huang, X. Chen, H. Mühlenbernd, H. Zhang, S. Chen, B. Bai, Q. Tan, G. Jin, K.-W. Cheah, C. W. Qiu, J. Li, T. Zentgraf, and S. Zhang, Three-dimensional optical holography using a plasmonic metasurface, *Nat. Commun.* **4**, 2808 (2013).
- [17] L. Li, T. J. Cui, W. Ji, S. Liu, J. Ding, X. Wan, B. L. Yun, M. Jiang, W. Q. Cheng, and S. Zhang, Electromagnetic reprogrammable coding-metasurface holograms, *Nat. Commun.* **8**, 197 (2017).
- [18] N. Yu, P. Genevet, M. A. Kats, F. Aieta, J. P. Tetienne, F. Capasso, and Z. Gaburro, Light propagation with phase

- discontinuities: Generalized laws of reflection and refraction, *Science* **334**, 333 (2011).
- [19] X. Li, L. Chen, Y. Li, X. Zhang, M. Pu, Z. Zhao, X. Ma, Y. Wang, M. Hong, and X. Luo, Multicolor 3D metaholography by broadband plasmonic modulation, *Sci. Adv.* **2**, e1601102 (2016).
- [20] D. Wen, F. Yue, G. Li, G. Zheng, K. Chan, S. Chen, M. Chen, K. F. Li, P. W. H. Wong, K. W. Cheah, E. Y. B. Pun, S. Zhang, and X. Chen, Helicity multiplexed broadband metasurface holograms, *Nat. Commun.* **6**, 8241 (2015).
- [21] B. O. Zhu and Y. Feng, Passive metasurface for reflectionless and arbitrary control of electromagnetic wave transmission, *IEEE Trans. Antennas Propag.* **63**, 5500 (2015).
- [22] S. M. A. M. H. Abadi and N. Behdad, Broadband true-time-delay circularly polarized reflectarray with linearly polarized feed, *IEEE Trans. Antennas Propag.* **64**, 4891 (2016).
- [23] X. Ding, F. Monticone, K. Zhang, L. Zhang, D. Gao, S. N. Burokur, A. Lustrac, Q. Wu, W. Q. Cheng, and A. Alù, Ultrathin Pancharatnam-Berry metasurface with maximal cross-polarization efficiency, *Adv. Mater.* **27**, 1195 (2015).
- [24] C. Pfeiffer, N. K. Emani, A. M. Shaltout, A. Boltasseva, V. M. Shalaev, and A. Grbic, Efficient light bending with isotropic metamaterial Huygens' surfaces, *Nano Lett.* **14**, 2491 (2014).
- [25] K. Chen, Y. Feng, F. Monticone, J. Zhao, B. Zhu, T. Jiang, L. Zhang, Y. Kim, X. Ding, S. Zhang, A. Alù, and W. Q. Cheng, A reconfigurable active Huygens' metalens, *Adv. Mater.* **29**, 1606422 (2017).
- [26] Z. Wang, X. Ding, K. Zhang, and Q. Wu, Spacial energy distribution manipulation with multi-focus Huygens metamirror, *Sci. Rep.* **7**, 9081 (2017).
- [27] A. Epstein, J. P. Wong, and G. V. Eleftheriades, Cavity-excited Huygens' metasurface antennas for near-unity aperture illumination efficiency from arbitrarily large apertures, *Nat. Commun.* **7**, 10360 (2016).
- [28] A. Epstein and G. V. Eleftheriades, Passive lossless Huygens metasurfaces for conversion of arbitrary source field to directive radiation, *IEEE Trans. Antennas Propag.* **62**, 5680 (2014).
- [29] C. Jin, M. Afsharnia, R. Berlich, S. Fasold, C. Zou, D. Arslan, I. Staude, T. Pertsch, and F. Setzpfandt, Dielectric metasurfaces for distance measurements and three-dimensional imaging, *Adv. Photon.* **1**, 036001 (2019).
- [30] Z. Wang, X. Ding, K. Zhang, B. Ratni, S. N. Burokur, X. Gu, and Q. Wu, Huygens metasurface holograms with the modulation of focal energy distribution, *Adv. Opt. Mater.* **6**, 1800121 (2018).
- [31] C. Pfeiffer and A. Grbic, Metamaterial Huygens' Surfaces: Tailoring Wave Fronts with Reflectionless Sheets, *Phys. Rev. Lett.* **110**, 197401 (2013).
- [32] M. Decker, I. Staude, M. Falkner, J. Dominguez, D. N. Neshev, I. Brener, T. Pertsch, and Y. S. Kivshar, High-efficiency dielectric Huygens' surfaces, *Adv. Opt. Mater.* **3**, 813 (2015).
- [33] See the Supplemental Material at <http://link.aps.org/supplemental/10.1103/PhysRevApplied.13.014033> for numerical post-processing of images and experimental section.
- [34] R. Di Leonardo, F. Ianni, and G. Ruocco, Computer generation of optimal holograms for optical trap arrays, *Opt. Express* **15**, 1913 (2007).
- [35] F. Zhou, Y. Liu, and W. Cai, Plasmonic holographic imaging with V-shaped nanoantenna array, *Opt. Express* **21**, 4348 (2013).
- [36] K. E. Chong, L. Wang, I. Staude, A. R. James, J. Dominguez, S. Liu, G. S. Subramania, M. Decker, D. N. Neshev, I. Brener, and Y. S. Kivshar, Efficient polarization-insensitive complex wavefront control using Huygens' metasurfaces based on dielectric resonant meta-atoms, *ACS Photonics* **3**, 514 (2016).
- [37] L. Wang, S. Kruk, H. Tang, T. Li, I. Kravchenko, D. N. Neshev, and Y. S. Kivshar, Grayscale transparent metasurface holograms, *Optica* **3**, 1504 (2016).
- [38] X. Li, H. Ren, X. Chen, J. Liu, Q. Li, C. Li, G. Xue, J. Jia, L. Cao, A. Sahu, and B. Hu, Athermally photoreduced graphene oxides for three-dimensional holographic images, *Nat. Commun.* **6**, 6984 (2015).
- [39] B. Walther, C. Helgert, C. Rockstuhl, F. Setzpfandt, F. Eilenberger, E. B. Kley, F. Lederer, A. Tünnermann, and T. Pertsch, Spatial and spectral light shaping with metamaterials, *Adv. Mater.* **24**, 6300 (2012).
- [40] B. Wang, F. Dong, Q. T. Li, D. Yang, C. Sun, J. Chen, Z. Song, L. Xu, W. Chu, Y. F. Xiao, and Q. Gong, Visible-frequency dielectric metasurfaces for multiwavelength achromatic and highly dispersive holograms, *Nano Lett.* **16**, 5235 (2016).
- [41] W. Zhao, H. Jiang, B. Liu, J. Song, Y. Jiang, C. Tang, and J. Li, Dielectric Huygens' metasurface for high-efficiency hologram operating in transmission mode, *Sci. Rep.* **6**, 30613 (2016).
- [42] X. Wan, Q. Zhang, T. Y. Chen, L. Zhang, W. Xu, H. Huang, C. K. Xiao, Q. Xiao, and T. J. Cui, Multichannel direct transmissions of near-field information, *Light-Sci. Appl.* **8**, 1 (2019).
- [43] A. C. Overvig, S. Shrestha, S.C. Malek, M. Lu, A. Stein, C. Zheng, and N. Yu, Dielectric metasurfaces for complete and independent control of optical amplitude and phase. arXiv preprint arXiv:1903.00578 (2019).